

Geophysical Research Letters

RESEARCH LETTER

10.1029/2020GL091554

Key Points:

- We discovered tissantite, a high-pressure mineral, in nine strongly shock-lithified lunar breccias
- We discovered Si-rich corundum in two strongly shock-lithified lunar breccias
- The high-pressure minerals provide constraints on the shock pressure and temperature during strong shock lithification of lunar regoliths

Supporting Information:

- Supporting Information S1

Correspondence to:







A.-C. Zhang,
aczhang@nju.edu.cn

Citation:

Zhang, A.-C., Jiang, Q.-T., Tomioka, N., Guo, Y.-J., Chen, J.-N., Li, Y., et al. (2021). Widespread tissantite in strongly shock-lithified lunar regolith breccias. *Geophysical Research Letters*, 48, e2020GL091554. <https://doi.org/10.1029/2020GL091554>

Received 3 NOV 2020
 Accepted 25 JAN 2021

Widespread Tissantite in Strongly Shock-Lithified Lunar Regolith Breccias

Ai-Cheng Zhang^{1,2} , Qin-Ting Jiang^{1,3}, Naotaka Tomioka⁴ , Yan-Jun Guo⁵ , Jia-Ni Chen¹, Yang Li^{2,6} , Naoya Sakamoto⁷ , and Hisayoshi Yurimoto^{7,8} 

¹State Key Laboratory for Mineral Deposits Research, School of Earth Science and Engineering, Nanjing University, Nanjing, China, ²CAS Center for Excellence in Comparative Planetology, Hefei, China, ³Now at Department of Geology & Geophysics, Yale University, New Haven, CT, USA, ⁴Kochi Institute for Core Sample Research, Japan Agency for Marine-Earth Science and Technology (JAMSTEC), Nankoku, Kochi, Japan, ⁵CAS Key Laboratory of Standardization and Measurement for Nanotechnology, CAS Center for Excellence in Nanoscience, National Center for Nanoscience and Technology, Beijing, China, ⁶Center for Lunar and Planetary Sciences, Institute of Geochemistry, Chinese Academy of Sciences, Guiyang, China, ⁷Isotope Imaging Laboratory, Creative Research Institution, Hokkaido University, Sapporo, Japan, ⁸Department of Natural History Sciences, Hokkaido University, Sapporo, Japan

Abstract Shock-lithification is a fundamental process of making rocks from fine-grained and porous regoliths on the surface of the Moon. Previous investigations have constrained potential shock pressures during shock-lithification based on experimental and numerical simulations. However, pressure and temperature conditions during shock-lithification have not been directly inferred from natural lunar breccias. Here, we report the discovery of widespread tissantite in strongly shock-lithified lunar meteorites, accompanied occasionally by Si-rich corundum and coesite. The coexistence of tissantite and coesite and the absence of stishovite in molten regions indicate a shock pressure of 4–8 GPa, which might be the pressure boundary between weak and strong shock-lithification. Meanwhile, the presence of Si-rich corundum imposes a temperature constraint of ~2,300 K for the intergranular melts. This temperature constraint has profound significance for interpreting the behaviors of volatile and moderately volatile elements and remanent magnetization records during strongly shock-lithification of lunar breccias.

Plain Language Summary It is widely accepted that high-speed impact makes lunar breccias from regolith on the Moon's surface. However, the detailed pressure and temperature conditions during strong shock lithification remain an open question due to complex properties and impact history of components in lunar breccias. In this study, we report the first discovery of tissantite, a high-pressure mineral, and Si-rich corundum in strongly shock-lithified lunar breccias. Using the high-pressure minerals in lunar breccias, we constrained the lower boundary (4–8 GPa) of shock pressure for strong shock lithification of lunar regoliths and the profound thermal effect.

1. Introduction

The surface of the Moon is covered mainly by fine-grained loose or consolidated materials, which are generally termed regoliths. The thickness of the regolith layer on the lunar surface varies from a few meters in the mare regions to tens of meters in the highlands regions (McKay et al., 1991; Spray, 2016). All the lunar materials (including mission-returned samples and lunar meteorites) available to be analyzed in laboratories up to date, and most of the in situ and remote-sensing data, are derived from these regoliths (McKay et al., 1991). Unraveling the components of these regoliths and their formation and evolution history is crucial in reconstructing the formation and evolution history of the Moon. Meanwhile, the physical properties of the regoliths (e.g., porosity and mechanical intensity) are also a key factor that should be considered for construction of lunar bases (Benaroya et al., 2002).

Shock-lithification has been considered as the most important physical process that makes dense regolith breccias from fine-grained and porous regolith materials on the Moon and asteroids (Bland et al., 2014; Kieffer, 1975; McKay et al., 1991; Spray, 2016). Shock-lithification of lunar regoliths has been divided into weak and strong shock-lithification, mainly involving mechanical compaction and formation of shock-induced intergranular glass, respectively (Christie et al., 1973; Kieffer, 1975). Weak shock-lithification mainly leads to a decrease of porosity, and its thermal effect might be limited. In contrast, strong shock-lithification

involves local or bulk melting of intergranular fine-grained materials. The shock-induced intergranular melt/glass would behave like an “adhesive” to coalesce mineral grains and fragments, enhancing the mechanical intensity of regolith breccias. Meanwhile, formation of shock-induced melt might have profound thermal effects. For instance, high temperatures during the formation of shock-induced melts may cause degassing of volatile and even moderately volatile elements (e.g., noble gases, Pb, K, and Zn) to various degrees, disturbance of U-Pb systematics of U-bearing minerals, and modification of remanent magnetization records in brecciated materials (Gibbons et al., 1975). Presence of the thermal effects makes precisely unraveling the clues of formation and evolution of the Moon very challenging. Therefore, it is critical to constrain qualitatively and quantitatively the thermal effects during strong shock-lithification of lunar regoliths.

In the past 5 decades, numerous experimental and theoretical investigations have been performed to constrain the scales of shock-induced pressure and temperature in porous materials (Bland et al., 2014; Christie et al., 1973; Hirata et al., 2009; Kieffer, 1975; McKay et al., 1991; Schaal & Hörz, 1980; Spray, 2016; Tomeoka et al., 1999; Wünnemann et al., 2008). It is generally accepted that low-velocity impact events respond to weak shock-lithification whereas high-velocity impact events lead to strong shock-lithification of regoliths (Christie et al., 1973; Kieffer, 1975; McKay et al., 1991; Spray, 2016). The extent of melting is a function of impact velocity and original porosity. High impact velocity and high porosity are favorable for melting of regoliths. However, a large discrepancy still exists for shock pressures during strong shock-lithification (Stöffler et al., 2018) and the reason remains unknown. Shock temperatures are even less understood due to heterogeneous distribution and lack of suitable temperature indicators. Meanwhile, mineral and lithic fragments in regoliths have various provenances, grain sizes, initial porosities, and impact histories. Except a few impact melt breccias (e.g., Zhang et al., 2011), up to date, pressure and temperature conditions during shock lithification have not been deduced directly based on mineralogical observations on brecciated lunar samples. It remains very challenging to constrain shock-lithification conditions by applying the data from shock recovery experiments on regolith analogs and theoretical simulations.

The phase transformation of a mineral is a function of pressure, temperature, time, and mineral composition. In the past decades, many high-pressure minerals have been discovered in meteorites and are widely used to constrain shock conditions of natural impact events (e.g., Gillet & El Goresy, 2013; Sharp & DeCarli, 2006; Tomioka & Miyahara, 2017). In lunar samples, a few high-pressure minerals, such as ringwoodite, xieite, coesite, stishovite, seifertite, and reidite, have been reported in unbrecciated samples and mineral fragments in lunar breccias (Fritz et al., 2020; Kaneko et al., 2015; Kayama et al., 2018; Miyahara et al., 2013; Ohtani et al., 2011; Xing et al., 2020; Zhang et al., 2010). However, no high-pressure minerals have previously been reported in the fine-grained matrix of lunar breccias. In the present study, we report on the presence of tissintite and Si-rich corundum in the shock-induced glassy matrix of a number of brecciated lunar meteorites. Tissintite is a vacancy-rich, high-pressure clinopyroxene with an anorthite-dominant plagioclase composition (Ma et al., 2015). The presence of tissintite and Si-rich corundum in lunar meteorites provides important mineralogical constraints on the pressure and temperature conditions during strong shock-lithification of lunar regoliths.

2. Analytical Methods

Petrographic textures of the lunar meteorites were observed using the Zeiss Supra55 field emission scanning electron microscope (FE-SEM) at Nanjing University, Nanjing, China. Some polished thick sections of the samples were also observed with a Nikon optical microscope in the reflected-light mode. The Zeiss FE-SEM instrument was operated at 15 kV accelerating voltage. A silicon drift energy dispersive detector (EDS) attached on the Zeiss FE-SEM instrument was also used to measure compositions of minerals and glass with 100 s measurement time and to map the distributions of different elements among various phases.

Chemical compositions of major and minor elements in tissintite and associated glass in a number of lunar meteorites were quantified using the JEOL JXA 8,100 electron probe micro-analyzer (EPMA) at Nanjing University. The EPMA instrument was operated at 15 kV accelerating voltage with a focused beam of 20 nA. Measurement times for elemental peak and background for most elements are 20 s and 10 s, respectively, except Na and K (10 s and 5 s for peak and background measurements, respectively). Natural and synthetic standards were used for concentration calibration. A natural hornblende standard was used for K, Na, Ca,

Mg, Ti, Al, and Si. A natural fayalite standard was used for Fe and Mn concentration calibration while a synthetic Cr_2O_3 oxide standard was used for Cr concentration calibration. All data have been reduced with the ZAF (atomic number-absorption-fluorescence) procedure. Typical detection limit for the EPMA analyses is better than 0.02 wt%.

Structural characterization of minerals and glass in the lunar meteorites were performed using a combination of Raman spectroscopy, electron backscatter diffraction (EBSD), and selected area electron diffraction (SAED). The Raman spectra of minerals and glass were collected using the Renishaw in via Plus microRaman spectrometer with a charge coupled device (CCD) detector at the National Center for Nanoscience and Technology of China, Beijing. The excitation laser wavelength is 514 nm and the laser power on the sample is ~ 10 – 12 mW. The laser spot size is ~ 1 μm . The measurement time varies from 20 to 60 s.

The EBSD patterns of minerals were collected using EBSD detectors installed on the JEOL 6490 and JEOL 7000F SEM instruments at Nanjing University, Nanjing, and Hokkaido University, Sapporo, Japan, respectively. Both EBSD detectors are controlled by the Aztec software. Before EBSD analysis, the polished sections were VibroMet polished and carbon-coated. During analysis, the EBSD pattern and EDS spectrum were obtained simultaneously. The EBSD analyses were performed at 20 kV accelerating voltage. A beam current of 4 nA was used for the analyses based on the JEOL 7000F SEM instrument. The collected EBSD patterns were indexed with potential phases for given constituent elements from both the HKL data set and a data set from the Mineralogical Society of America. The indexed results with mean angular deviation (MAD) values less than one are considered as reasonable structural solutions.

The focused ion beam (FIB) technique was employed to prepare two foils for observations using a transmission electron microscope (TEM). Cutting and thinning of the two foils were conducted using the FEI Scios FIB-SEM instrument at the Institute of Geochemistry, Chinese Academy of Sciences, Guiyang, China. An accelerating voltage of 30 kV and various ion beam currents of 15 nA–300 pA were used. The final thickness of the two FIB foils is ~ 100 nm. The observations and analyses on the two FIB foils were carried out using the FEI Tecnai F20 TEM instrument at Nanjing University. The F20 TEM instrument was conducted at an accelerating voltage of 200 kV. The foils were observed under both conventional TEM and high-angle annular dark-field scanning transmission electron microscopy (HAADF-STEM) modes. The minerals were identified using SAED. Chemical compositions of the phases in the foils were measured using an energy dispersive X-ray detector (EDS) installed on the F20 TEM instrument in STEM mode. The k-factors for quantitative STEM-EDS analysis were calibrated by comparing average SEM-EDS and STEM-EDS data on glass surrounding tissintite and corundum grains.

3. Results

In this study, we have performed petrographic and mineralogical observations on 12 brecciated lunar meteorites: Northwest Africa (abbreviated as NWA hereafter) 2995, NWA 5000, NWA 8182, NWA 10203, NWA 10901, NWA 10253, NWA 10272, NWA 10782, NWA 11212, NWA 11228, NWA 11273, and NWA 11474. All these lunar meteorites are dominated by feldspathic components, although basaltic components are also present with various abundance in some of these samples. Nine of the 12 lunar meteorites contain abundant glass infilling the interstices between mineral and lithic fragments. The other three meteorites (NWA 11212, NWA 11228, and NWA 11474) show no obvious molten features between mineral and lithic fragments or only contain very few short and thin melt veins (~ 10 μm in thickness), although glassy fragments could be present.

Tissintite is commonly observed with various abundances in the nine lunar meteorites containing glassy regions (Figure 1, S1, and S2), but absent in the three lunar meteorites without obvious molten features. This mineral typically occurs as fine-grained clusters embedded in the intergranular glass, which, in reflected light, appears to be interconnected with each other (Figure S1). In NWA 5000, the tissintite clusters not only occur in the intergranular glassy regions (Figure S2i), but also occur in typical shock melt veins that are straight and cutting through mineral and lithic fragments (Figure S2j). The tissintite clusters in this study typically form a zone of ~ 2 – 30 μm wide at the interfaces between glassy regions and surrounding unmelted materials (Figures 1a, 1b, and S2). Some tissintite clusters nucleate from the margin of relict, unmelted

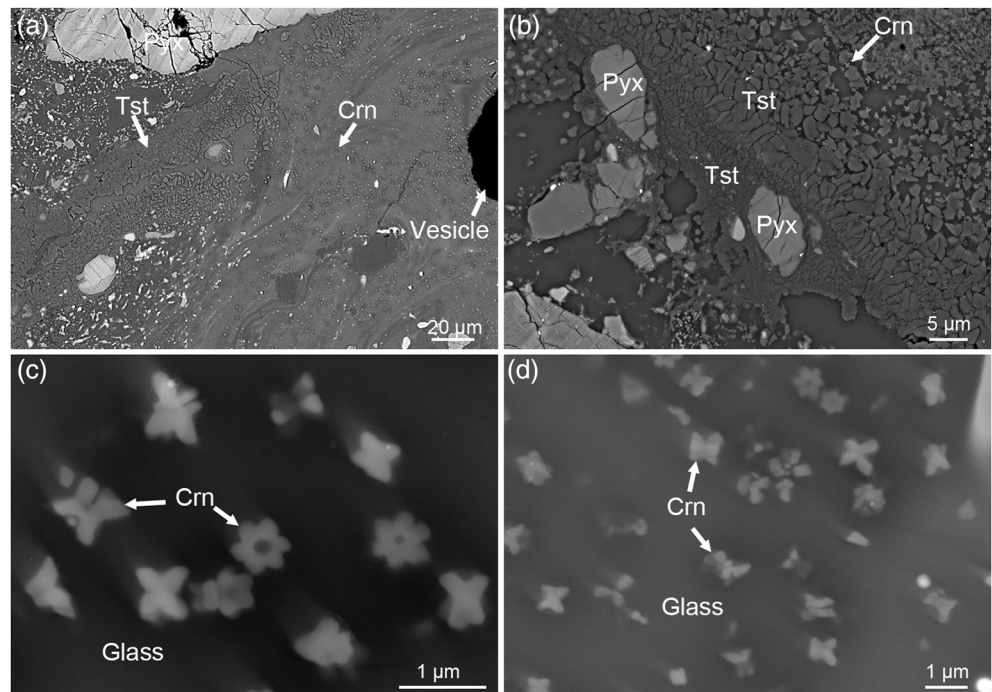


Figure 1. Backscattered electron images of tissantite and corundum in lunar meteorite NWA 2995. (a) A typical thick glassy region with tissantite aggregates at the edge zone and corundum grains dispersed at the center zone. (b) At the edge zone, Mg,Fe-poor and Mg,Fe-bearing tissantite aggregates are in contact. At the center zone, both corundum and Mg,Fe-bearing tissantite are present. (c and d) Flower-like corundum aggregates are located in glass. Crn, Corundum; NWA, Northwest Africa; Pyx, Pyroxene; Tst, Tissantite.

pyroxene fragments in the glassy regions (Figure 1b). In some of the tissantite-bearing glassy regions, coesite is present, occasionally associated with moganite (Figures S3 and S4). However, neither stishovite nor seifertite is present based on our textural observations in BSE mode and Raman and EBSD measurements. Although fragments of pyroxene, olivine, and apatite are present in the tissantite-bearing regions, none of their high-pressure polymorph was observed. Vesicles are commonly present within the thick glassy regions containing tissantite except in NWA 5000, and their sizes vary from submicron to $\sim 200 \mu\text{m}$ in length (Figure S1).

The crystal structure of tissantite is confirmed by laser Raman, EBSD, and SAED analyses (Figures S5–S7). Chemically, tissantite in the lunar meteorites has a large variation among different regions and samples. The MgO and FeO contents vary from 0.3 wt% to 6.7 wt% and from 0.3 wt% to 7.4 wt%, respectively and are essentially identical to the compositions of surrounding glass (e.g., Table S1). However, it is noteworthy that in four of the samples (NWA 2995, NWA 10253, NWA 10272, and NWA 10782), Mg,Fe-poor tissantite in anorthite glass is in direct contact with Mg,Fe-bearing/rich tissantite (Figure 1b), with the MgO + FeO contents ($>1 \text{ wt}\%$) higher than that of anorthite (Table S1).

In NWA 2995 and NWA 10203, a few glassy regions as thick as up to hundreds of micrometers show mineralogical zoning from the edge to the inner zone. At the edge, tissantite is the predominant crystalline phase while innerward to the inner zone corundum is observed (Figures 1 and S1). In some regions, both corundum and tissantite are present in glass (Figure 1b). The corundum usually occurs as submicron-sized flower-like aggregates (Figures 1c and 1d). The crystal structure of corundum is determined by EBSD and SAED (Figures S5, S6c and S6d). The chemical compositions of corundum grains are determined by STEM-EDS. Given the small grain size of corundum in this study, beam overlapping with surrounding glass is inevitable during STEM-EDS analyses. We calculate the corundum composition by attributing all the measured CaO concentrations to the contamination from surrounding glass. After subtracting the contribution from glass and normalization to 100 wt%, the corundum grains contain 90.7–93.9 wt% Al_2O_3 with 4.4–6.8 wt% SiO_2 and 1.6–2.2 wt% MgO + FeO (Table S2).

4. Discussion

4.1. Formation Conditions of Tissintite and Corundum

Tissintite has been reported previously in basaltic Martian meteorites (shergottites) and eucrite meteorites. Most of the tissintite grains in these meteorites occur as fine-grained clusters in shock-induced plagioclase glass or at the margins of plagioclase glass adjacent to shock melt veins or pockets (D. L. Chen et al., 2019; Ma et al., 2015; Pang et al., 2016; Walton et al., 2014). These tissintite grains have a composition essentially identical to that of the adjacent plagioclase glass. The occurrences indicate nucleation and growth of tissintite from high-pressure plagioclase glass (D. L. Chen et al., 2019; Ma et al., 2015; Pang et al., 2016), although the exact formation mechanism of the plagioclase glass (diaplectic glass vs. quenched high-pressure melt) is still an issue of controversy (M. Chen & El Goresy, 2000; D. L. Chen et al., 2019; Yamaguchi & Sekine, 2000). Recently, Mg,Fe-rich tissintite has also been reported in a shock melt vein from a shocked shergottite (Ma & Beckett, 2017). In the present study, tissintite is first reported in lunar samples. Most of them are Mg,Fe-bearing/rich tissintite as fine-grained clusters in the intergranular melts in regolith breccias, with minor Mg,Fe-poor tissintite present at the margins of shock-induced plagioclase glass.

Although the experimental investigation by Rucks et al. (2018) suggested that tissintite can form from plagioclase glass during decompression, natural tissintite has been mainly explained as a crystallization phase from a high-pressure melt (D. L. Chen et al., 2019; Ma & Beckett, 2017; Ma et al., 2015; Pang et al., 2016). This melt-crystallization model can account for the formation of tissintite in lunar meteorites as well. Two observations in the present study support this inference. First, all the tissintite in the lunar meteorites occurs as fine-grained clusters or overgrowth crystals on relict pyroxene grains in the formerly molten regions, generally similar to those in Martian and eucrite meteorites (D. L. Chen et al., 2019; Ma & Beckett, 2017; Ma et al., 2015; Pang et al., 2016). Second and more importantly, most of the tissintite grains in the lunar meteorites contains higher MgO + FeO contents (>1 wt%) than anorthite (Table S1), indicating various contribution from mafic phases, and therefore a mixed composition melt of plagioclase composition with contributions from pyroxene and/or olivine. Meanwhile, the essentially identical chemical compositions between tissintite and surrounding glass indicate no chemical equilibration between tissintite and surrounding melt during the crystallization of tissintite. This feature can be interpreted with rapid crystallization of tissintite, consistent with its metastable origin (Ma et al., 2015). For most cases in the present study, tissintite is the only phase that crystallized from the formerly molten regions and melt veins. Given the hypothesis that high-pressure minerals probably started crystallization from the melts during shock pressure decline (Fritz et al., 2017), therefore, the crystallization pressure of tissintite can be considered as the minimum peak shock pressure for the melt-forming impact event (Fritz et al., 2017; Sharp & DeCarli, 2006).

Corundum is a relatively rare mineral in extraterrestrial samples. Its formation varies from presolar origin (Takigawa et al., 2018), solar-nebula condensation origin (Makide et al., 2009; Simon et al., 2002), alteration origin of Ca,Al-rich inclusions (Ma et al., 2009), xenolith origin in eucritic basalt (Li et al., 2020), shock-induced origin (Pang et al., 2018, 2019; Yang et al., 2019), and unknown origin (Christophe-Michel-Levy et al., 1972; Kleinmann & Ramdohr, 1971). In the Apollo samples, corundum grains were found only in fines, without exact textural information (Christophe-Michel-Levy et al., 1972; Kleinmann & Ramdohr, 1971). The Apollo corundum grains are almost pure alumina and vary from 40 to 200 μm in size. Such a relatively large grain size might exclude a shock-induced origin of these Apollo corundum grains, since most shock-induced minerals are usually fine-grained (<5 μm in size; Sharp & DeCarli, 2006; Tomioka & Miyahara, 2017). In the present study, corundum occurs as a fine-grained aggregate dispersed in the inner part of shock-induced melt regions which contains the high-pressure mineral tissintite. This occurrence and the association with tissintite indicate that the corundum aggregates formed from a shock-induced melt in the lunar meteorites, similar to that in the eucrite NWA 8003 (Pang et al., 2018, 2019) and the achondrite meteorite NWA 7325 (Yang et al., 2019), but different from the corundum grains (40–200 μm in size) in Apollo fines (Christophe-Michel-Levy et al., 1972; Kleinmann & Ramdohr, 1971). In texture, tissintite is located at the edge of the zoned, molten regions while corundum is located at the inner zone (Figure 1). Considering thermal conductivity from the shock-induced melt to the unmelted host rock, the inner zone of the molten regions should have a lower cooling rate compared with the edge (Sharp & DeCarli, 2006). Therefore, corundum might have formed at pressure and temperature conditions similar to or relatively lower than that for tissintite at the edges.

Tissintite of Ca-rich plagioclase composition has been reported in shocked meteorites with bulk shock pressures ranging from ~ 10 GPa to >19 GPa, which are constrained from the plagioclase-maskelynite transformation, the deformation in mafic minerals, and the stability of high-pressure minerals (D. L. Chen et al., 2019; Ma et al., 2015; Pang et al., 2016; Walton et al., 2014). In these meteorites, tissintite occurs along the boundary between shock melt veins and host rock or in the margins of plagioclase glass in contact with quenched shock melt. If tissintite crystallized during shock pressure decline (Fritz et al., 2017), it might have formed at ~ 10 – 19 GPa or a lower pressure (Pang et al., 2016). Rucks et al., (2018, 2019) observed the presence of tissintite with a composition An_{40-80} in their synthetic samples at a pressure of 4.5–10 GPa and a temperature of >1273 K. However, no tissintite was observed at a pressure below ~ 3 GPa (Rucks et al., 2018, 2019). Therefore, 4–5 GPa might be the lower limit for the tissintite formation of Ca-rich plagioclase composition (Rucks et al., 2019). Although most tissintite grains in the lunar meteorites contain a few weight percent of MgO + FeO (>1 wt%) differing from the Mg,Fe-poor tissintite in the synthetic experiments (Rucks et al., 2018, 2019), some of the Mg,Fe-bearing/rich tissintite aggregates are in direct contact spatially with Mg,Fe-poor tissintite in chemically heterogeneous molten regions (Figure 1b). Therefore, it is likely that the Mg,Fe-bearing tissintite aggregates have also formed at a pressure at least 4–5 GPa.

Coesite and stishovite are two high-pressure polymorphs of silica. These two minerals have different solid-state phase transformation behaviors. The solid-state transformation from quartz to coesite at >2.5 GPa is sluggish due to a high kinetic barrier (D. L. Chen et al., 2019; Miyahara et al., 2014; Pang et al., 2016). However, the solid-state transformation from low-pressure silica phases to stishovite could be very fast. For example, stishovite can form within $1 \mu\text{s}$ from quartz with a shock pressure >7.5 GPa (Mansfeld et al., 2017). If the starting material is fused silica, the transformation to stishovite would be much fast (~ 1.4 ns) during compression (Gleason et al., 2015). In the present study, in tissintite-rich glassy regions, coesite was observed in irregularly shaped silica aggregates (Figure S3). The occurrence is distinctly different from the euhedral coesite grains that crystallized from shock-induced melts (e.g., D. L. Chen et al., 2019; Pang et al., 2016). This feature implies that the coesite grains in the present study have formed through solid-state phase transition during shock metamorphism (Kayama et al., 2018). Considering the ultrafast transformations from low-pressure silica phases to stishovite demonstrated experimentally (Gleason et al., 2015; Mansfeld et al., 2017), stishovite would be expected to promptly form if the shock pressure reached its lower stability limit. The fact that no stishovite was detected in our study suggests peak shock pressures in lunar regolith breccias did not exceed ~ 8 GPa. Recently, Fritz et al. (2017) argued that the peak shock pressure for bulk rock during shock metamorphism should be higher than the pressures deduced from the stability of high-pressure minerals. Fritz's argument was based on the assumption that most of shocked meteorites are derived from the region outside of isobaric cores of impact events and do not experience broad pressure plateaus, therefore, high-pressure minerals usually crystallize during decompression (Fritz et al., 2017). However, the results of above-mentioned shock experiments (Gleason et al., 2015; Mansfeld et al., 2017) suggest stishovite can rapidly grow in its stability pressures even if shock pressure duration is less than microseconds. In this study, therefore, we propose that 8 GPa might be the upper limit for the shock pressure based on the absence of stishovite. If it is the case, the tissintite-rich glassy regions probably have formed at a shock pressure around 4–8 GPa.

The corundum in this study is characterized by its high contents of SiO_2 (up to ~ 7 wt%). Based on our knowledge, it is the first report of Si-rich corundum in lunar samples. In the corundum structure, Al ions occupy the oxygen octahedral sites. Incorporation of Si into the corundum structure implies that Si ions probably substitute the $^{\text{VI}}\text{Al}$ ions, requiring high-pressure formation conditions similar to the cases of stishovite and supersilicic garnet (D. L. Chen et al., 2019; Pang et al., 2016). The phase diagram of anorthite composition at high P-T conditions indicates that corundum can occur at a high temperature $>1,673$ K and a wide range of pressure from <1 GPa to ~ 15 GPa (X. Liu et al., 2012). However, no phase diagram involving crystallization of Si-rich corundum in a melt of feldspathic composition has been reported to date. Here, we employ the phase diagram in the system $\text{MgSiO}_3\text{-Al}_2\text{O}_3$ at high pressure and high temperature to roughly constrain the formation condition of Si-rich corundum (Z. D. Liu et al., 2017). According to the $\text{MgSiO}_3\text{-Al}_2\text{O}_3$ phase diagram (Figure 9 of Z. D. Liu et al., 2017), corundum can contain some amount of MgSiO_3 component at temperatures $>1,700$ K and pressures $>\sim 15$ GPa. At these pressures, higher temperature corundum can contain a larger amount of Mg and Si as the $^{\text{VI}}(\text{Mg,Si})_2\text{O}_3$ component. Assuming a 10 mol% MgSiO_3 component in corundum, only when the temperature reached $\sim 2,300$ K the pressure would be comparable to

the shock pressure (4–8 GPa) deduced above. Additionally, if the temperature was less than $\sim 1,900$ and $\sim 2,300$ K for a pressure of 4 and 8 GPa, respectively, grossular and/or kyanite would be present as one of the stable phases for an anorthitic melt (X. Liu et al., 2012). Shock-induced mineral assemblages containing corundum + kyanite and grossular + kyanite have been reported in the eucrite meteorites containing tissintite (D. L. Chen et al., 2019; Pang et al., 2019). However, no grossular and kyanite were observed in the present study. Therefore, the absence of grossular and kyanite can be considered as another piece of evidence suggesting a high temperature $> 2,300$ K. Therefore, the temperature 2,300 K might represent the lower limit of the shock high temperature in the Si-rich corundum-bearing melt.

In summary, the glass containing tissintite and Si-rich corundum in the nine lunar meteorites might have formed at a shock pressure of the 4–8 GPa level and reached a high temperature at least up to 2,300 K.

4.2. Implications for Strong Shock-Lithification of Lunar Regoliths

Shock-induced intergranular melting and recrystallization is an important feature for classifying weak and strong shock-lithification of lunar regoliths (Kieffer, 1975). Based on this criterion, the nine lunar meteorites in this study with molten regions and high-pressure minerals therein are strongly shock-lithified lunar breccias; however, the meteorites NWA 11212, NWA 11228, and NWA 11474 represent three weakly shock-lithified lunar breccias.

There are two ways to constrain the pressure and temperature conditions during shock-lithification of regolith breccias. One is based on the shock-induced effects in mineral and lithic fragments, such as fractures, deformation, phase transformation, decomposition, and/or melting (Stöffler et al., 2018). The other is based on the intergranular glass between mineral and lithic fragments. However, mineral and lithic fragments in lunar regolith breccias may have different provenances and complex shock histories (Stöffler et al., 2018). It is likely that the complex shock-induced effects in mineral and lithic fragments cannot unambiguously reflect the lithification shock event. Meanwhile, most of the mineral and lithic fragments in lunar regolith breccias are usually fine-grained. The shock-induced effects cannot be readily identified. Therefore, it is difficult to constrain the shock-lithification conditions of lunar regoliths by using shock-induced effects in mineral and lithic fragments. Rather, the formation conditions of strongly shock-lithified regolith breccias can be inferred from the formation conditions of the shock-induced intergranular melts, which can be constrained based on the pressure-temperature stability of minerals that have crystallized from the melts (e.g., Sharp & DeCarli, 2006).

Based on the current observations, all of the nine strongly shock-lithified regolith breccias contain tissintite in the shock-induced intergranular glass. However, no tissintite was observed in the three weakly shock-lithified regolith breccias. It is reasonable to infer that formation conditions of the tissintite-bearing intergranular glass probably represent the boundary conditions between weak and strong shock-lithification of lunar regoliths. Based on the above discussion, the 4–8 GPa shock pressure might be the pressure boundary between weak and strong shock-lithification of lunar regoliths. This inferred shock pressure is consistent with the shock pressure (~ 5 GPa) inferred in Kieffer (1971) based on shock-lithified Coconino Sandstone samples at Meteor Crater, but much lower than that (~ 17 GPa) inferred in Schaal and Hörz (1980) based on shock-recovery experiments of the lunar soil 15101. The exact origin of this discrepancy for the pressure boundary inferred based on natural samples and shock-recovery experiments remains unknown. It might be related to a series of factors, such as the duration of shock pulses, mineral assemblage (anorthite-rich vs. olivine/pyroxene-rich), grain size, and porosity of natural lunar regoliths and their analogs in shock-recovery experiments. For instance, the durations of shock pulses in natural samples could be as long as tens of milliseconds to several seconds (Beck et al., 2005; M. Chen et al., 1996; Ohtani et al., 2004; Xie et al., 2006), while those in shock-recovery experiments can last only up to microseconds (DeCarli et al., 2002). This difference would influence overall shock petrography of lunar regolith breccias, if considering that many of the shock-induced effects are not only pressure-dependent but also kinetically controlled.

It is widely accepted that the shock-induced temperature increase is appreciable in high porous materials than that in less porous materials (Christie et al., 1973; Kieffer, 1971; Sharp & DeCarli, 2006; Stöffler et al., 2018; Wünnemann et al., 2008). Previous investigations have considered potential temperature in-

creases in shocked porous samples (Ahrens & Gregson, 1964; Christie et al., 1973; Kieffer, 1971). It was suggested that the temperature increases for bulk rocks could be as high as 1,273 K for a shock pressure of 5 GPa (Christie et al., 1973). However, the temperatures for intergranular melts, which are also important to understand the annealing effects in strongly shock-lithified breccias (Christie et al., 1973; Spray, 2016), were less well constrained. Recently, Bland et al. (2014) performed numerical simulations on the distribution of pressure and temperature in shocked chondritic meteorites. Based on their simulation results, high temperature heterogeneity (>1,000 K) could be present over ~100 μm . For shock pressures of 3 and 8 GPa, the local temperature in matrix with initial matrix porosity of 70% could be high up to 1,800 K and 3,300 K, respectively (Bland et al., 2014). The shock pressure and temperature conditions appear generally consistent with the high-temperature and high-pressure conditions inferred for the strongly shock-lithified lunar regoliths in the present study.

The very high temperature inferred for the intergranular melts might have caused release of trapped volatile from lunar regoliths, which was supported by the common presence of vesicles in the shock-induced glass in strongly lithified lunar meteorites (Figures S1 and S2). Given this profound thermal effect, many elemental and isotopic features of volatile and moderate volatile elements in lunar breccias might have been modified during strong shock-lithification events, at least in fine-grained and porous regions. It should be cautioned to infer the primary elemental and isotopic features of Moon only based on the strongly lithified lunar breccias. In addition, the shock temperatures for the intergranular melts are much higher than the Curie points of most materials (e.g., 1,053 K for kamacite; Mighani et al., 2020). Therefore, remanent magnetization records of the molten matrix should have been totally modified during strong shock-lithification of lunar regoliths, as suggested by previous investigations (e.g., Gibbons et al., 1975; Mighani et al., 2020).

5. Conclusions

We performed a petrographic and mineralogical study of 12 brecciated lunar meteorites. In the nine strongly shock-lithified breccias, which contain obvious shock-induced vesicle-bearing glassy regions, tissintite was observed for the first time. Coesite and Si-rich corundum were also observed closely associated with tissintite. However, no other high-pressure minerals were observed being associated with tissintite in the studied lunar breccias. The high-pressure mineral assemblage provides a quantitative constraint on the shock pressure and temperature for the formation of shock-induced intergranular melts, 4–8 GPa and up to 2,300 K, respectively. The 4–8 GPa shock pressure might be the lower limit for strong shock lithification of lunar regoliths. The high shock-induced high temperature is important for interpreting geochemical behaviors of volatile and moderate volatile elements and remanent magnetization records in strongly shock-lithified lunar breccias.

Data Availability Statement

The data reported in this work can be found in the supporting information and <http://dx.doi.org/10.17632/syjc87h62s.1>.

References

- Ahrens, T. J., & Gregson, V. G. (1964). Shock compression of crustal rocks. *Journal of Geophysical Research*, 69, 4839–4874. <https://doi.org/10.1029/JZ069i022p04839>
- Beck, P., Gillet, P., El Goresy, A., & Mostefaoui, S. (2005). Timescales of shock processes in chondritic and martian meteorites. *Nature*, 435, 1071–1074. <https://doi.org/10.1038/nature03616>
- Benaroya, H., Bernold, L., & Chua, K. M. (2002). Engineering, design and construction of lunar bases. *Journal of Aerospace Engineering*, 15, 33–45. [https://doi.org/10.1061/\(ASCE\)0893-1321](https://doi.org/10.1061/(ASCE)0893-1321)
- Bland, P. A., Collins, G. S., Davison, T. M., Abreu, N. M., Ciesla, F. J., Muxworthy, A. R., et al. (2014). Pressure-temperature evolution of primordial solar system solids during impact-induced compaction. *Nature Communications*, 5, 5451. <https://doi.org/10.1038/ncomms6451>
- Chen, D. L., Zhang, A. C., Pang, R. L., Chen, J. N., & Li, Y. (2019). Shock-induced phase transformation of anorthitic plagioclase in the eucrite meteorite Northwest Africa 2650. *Meteoritics & Planetary Sciences*, 54, 1548–1562. <https://doi.org/10.1111/maps.13286>
- Chen, M., & El Goresy, A. (2000). The nature of maskelynite in shocked meteorites: Not diaplectic glass but a glass quenched from shock-induced dense melt at high pressure. *Earth and Planetary Science Letters*, 179, 489–502. [https://doi.org/10.1016/S0012-821X\(00\)00130-8](https://doi.org/10.1016/S0012-821X(00)00130-8)

Acknowledgments

We appreciate the comments and suggestions by Dr. Erin Walton and an anonymous reviewer, and the editorial effort from AE Dr. Andrew J. Dombard. This work was supported by the B-type Strategic Priority Program of the Chinese Academy of Sciences (XDB41000000), the prereseach Project on Civil Aerospace Technologies funded by CNSA (D020204), and National Natural Science Foundation of China (42025302, 41973061, 41673068).

- Chen, M., Sharp, T. G., El Goresy, A., Wopenka, B., & Xie, X. (1996). The majorite-pyrope + magnesiowüstite assemblage: Constraints on the history of shock veins in chondrites. *Science*, *271*, 1570–1573. <https://doi.org/10.1126/science.271.5255.1570>
- Christie, J. M., Griggs, D. T., Heuer, A. H., Nord, G. L., Radcliffe, S. V., Lally, J. S., et al. (1973). Electron petrography of Apollo 14 and 15 breccias and shock-produced analogs. *Proceedings of the Fourth Lunar Science Conference*, *1*, 365–382.
- Christophe-Michel-Levy, M., Levy, C., Caye, R., & Pierrot, R. (1972). The magnesian spinel-bearing rocks from the Fra Mauro formation. *Proceedings of the Third Lunar Science Conference*, *1*, 887–894.
- DeCarli, P. S., Bowden, E., Sharp, T. G., Jones, A. P., & Price, G. D. (2002). Evidence for kinetic effects on shock wave propagation in tectonites. In M. D. Furnish, Y. M. Gupta, & J. W. Forbes (Eds.), *Shock compression of condensed matter—2001*. (pp. 1381–1384). Melville, NY: American Institute of Physics. <https://doi.org/10.1063/1.1483796>
- Fritz, J., Grechake, A., & Fernandes, V. A. (2017). Revising the shock classification of meteorites. *Meteoritics & Planetary Science*, *52*(6), 1216–1232.
- Fritz, J., Greshake, A., Klementova, M., Wirth, R., Palatinus, L., Trønnes, R. G., et al. (2020). Donwilhelmsite, $[\text{CaAl}_2\text{Si}_2\text{O}_{11}]$, a new lunar high-pressure Ca-Al-silicate with relevance for subducted terrestrial sediments. *American Mineralogist*, *105*, 1704–1711. <https://doi.org/10.2138/am-2020-7393>
- Gibbons, R. V., Morris, R. V., Hörz, F., & Thompson, T. D. (1975). Petrographic and ferromagnetic resonance studies of experimentally shocked regolith analogs. *Proceedings of the Sixth Lunar Science Conference*, *3*, 3143–3171.
- Gillet, P., & El Goresy, A. (2013). Shock events in the Solar System: The message from minerals in terrestrial planets and asteroids. *Annual Review of Earth and Planetary Sciences*, *41*, 257–285. <https://doi.org/10.1146/annurev-earth-042711-105538>
- Gleason, A. E., Bolme, C. A., Lee, H. J., Nagler, B., Galtier, E., Milathianaki, D., et al. (2015). Ultrafast visualization of crystallization and grain growth in shock-compressed SiO_2 . *Nature Communications*, *6*, 1–6. <https://doi.org/10.1038/ncomms9191>
- Hirata, N., Kurita, K., & Sekine, T. (2009). Simulation experiments for shocked primitive materials in the Solar System. *Physics of the Earth and Planetary Interiors*, *174*, 227–241. <https://doi.org/10.1016/j.pepi.2008.09.016>
- Kaneko, S., Miyahara, M., Ohtani, E., Arai, T., Hirao, N., & Sato, K. (2015). Discovery of stishovite in Apollo 15299 sample. *American Mineralogist*, *100*, 1308–1311. <https://doi.org/10.2138/am-2015-5290>
- Kayama, M., Tomioka, N., Ohtani, E., Seto, Y., Nagaoka, H., Götze, J., et al. (2018). Discovery of moganite in a lunar meteorite as a trace of H_2O ice in the Moon's regolith. *Science Advances*, *4*, eaar4378. <https://doi.org/10.1126/sciadv.aar4378>
- Kieffer, S. W. (1971). Shock metamorphism of the Coconino sandstone at Meteor Crater, Arizona. *Journal of Geophysical Research*, *76*, 5449–5473. <https://doi.org/10.1029/JB076i023p05449>
- Kieffer, S. W. (1975). From regolith to rock by shock. *The Moon*, *13*, 301–320. <https://doi.org/10.1007/BF00567522>
- Kleinmann, B., & Ramdohr, P. (1971). α -corundum from the lunar crust. *Earth and Planetary Science Letters*, *13*, 19–22.
- Li, J. Y., Zhang, A. C., Sakamoto, N., Yurimoto, H., & Gu, L. X. (2020). A new occurrence of corundum in eucrite and its significance. *American Mineralogist*, *105*, 1656–1661. <https://doi.org/10.2138/am-2020-7361>
- Liu, X., Ohfuji, H., Nishiyama, N., He, Q., Sanehira, T., & Irifune, T. (2012). High-P behavior of anorthite composition and some phase relations of the $\text{CaO-Al}_2\text{O}_3\text{-SiO}_2$ system to the lower mantle of the Earth, and their geophysical implications. *Journal of Geophysical Research*, *117*, B09205. <https://doi.org/10.1029/2012JB009290>
- Liu, Z. D., Nishi, M., Ishii, T., Fei, H., Miyajima, N., Ballaran, T. B., et al. (2017). Phase relations in the system $\text{MgSiO}_3\text{-Al}_2\text{O}_3$ up to 2300 K at lower mantle pressures. *Journal of Geophysical Research: Solid Earth*, *122*, 7775–7788. <https://doi.org/10.1002/2017JB014579>
- Ma, C., & Beckett, J. R. (2017). A new type of tissintite, $(\text{Ca,Mg,Na}_{0.14})(\text{Al,Fe,Mg})\text{Si}_2\text{O}_6$, in the Zagami martian meteorite: A high-pressure clinopyroxene formed in shock. In *48th Lunar and Planetary Science* (pp. 1639). The Woodlands, Texas. Conference Abstract #1639
- Ma, C., Simon, S. B., Rossman, G. R., & Grossman, L. (2009). Calcium Tshermak's pyroxene, CaAlAlSiO_6 , from the Allende and Murray meteorites: EBSD and micro-Raman characterizations. *American Mineralogist*, *94*, 1483–1486. <https://doi.org/10.2138/am.2009.3231>
- Ma, C., Tschauner, O., Beckett, J. R., Liu, Y., Rossman, G. R., Zhuravlev, K., et al. (2015). Tissintite $(\text{Ca,Na}_{0.1})\text{AlSi}_2\text{O}_6$, a highly-defective, shock-induced, high-pressure clinopyroxene in the Tissint Martian meteorite. *Earth and Planetary Science Letters*, *422*, 194–205. <https://dx.doi.org/10.1016/j.epsl.2015.03.057>
- Makide, K., Nagashima, K., Krot, A. N., & Huss, G. R. (2009). Oxygen isotopic components of solar corundum grains. *The Astrophysical Journal*, *706*, 142–147. <https://doi.org/10.1088/0004-637X/706/1/142>
- Mansfeld, U., Langenhorst, F., Ebert, M., Kowitz, A., & Schmitt, R. T. (2017). Microscopic evidence of stishovite generated in low-pressure shock experiments on porous sandstone: Constraints on its genesis. *Meteoritics & Planetary Sciences*, *52*, 1449–1464. <https://doi.org/10.1111/maps.12867>
- McKay, D. S., Heiken, G. H., Basu, A., Blanford, G., Simon, S., Reedy, R., et al. (1991). The lunar regolith. In G. H. Heiken, D. T. Vaniman, & B. M. French (Eds.), *Lunar Sourcebook—a user's guide to the Moon*. (pp. 285–356). Cambridge University Press.
- Mighani, S., Wang, H., Shuster, D. L., Borlina, C. S., Nichols, C. I. O., & Weiss, B. P. (2020). The end of the lunar dynamo. *Science Advances*, *6*, eaax0883. <https://doi.org/10.1126/sciadv.aax0883>
- Miyahara, M., Kaneko, S., Ohtani, E., Sakai, T., Nagase, T., Kayama, M., et al. (2013). Discovery of seifertite in a shocked lunar meteorite. *Nature Communications*, *4*, 1737. <https://doi.org/10.1038/ncomms2733>
- Miyahara, M., Ohtani, E., Yamaguchi, A., Ozawa, S., Sakai, T., & Hirao, N. (2014). Discovery of coesite and stishovite in eucrite. *Proceedings of the National Academy of Sciences of the United States of America*, *111*, 10939–10942. <https://doi.org/10.1073/pnas.1404247111>
- Ohtani, E., Kimura, Y., Kimura, M., Takata, T., Kondo, T., & Kubo, T. (2004). Formation of high-pressure minerals in shocked L6 chondrite Yamato 791384: Constraints on shock conditions and parent body size. *Earth and Planetary Science Letters*, *227*, 505–515. <https://doi.org/10.1016/j.epsl.2004.08.018>
- Ohtani, E., Ozasa, S., Miyahara, M., Ito, Y., Mikouchi, T., Kumura, M., et al. (2011). Coesite and stishovite in a shocked lunar meteorite, Asuka-881757, and impact events in lunar surface. *Proceedings of the National Academy of Sciences of the United States of America*, *108*, 463–466. <https://doi.org/10.1037/pnas.1009338108>
- Pang, R. L., Harries, D., Pollok, K., Zhang, A. C., & Langenhorst, F. (2018). Vestaitite, $(\text{Ti}^{++}\text{Fe}^{2+})\text{Ti}^{4+}_2\text{O}_6$, a new mineral in the shocked eucrite Northwest Africa 8003. *American Mineralogist*, *103*, 1502–1511. <https://doi.org/10.2138/am-2018-6522>
- Pang, R. L., Harries, D., Pollok, K., Zhang, A. C., & Langenhorst, F. (2019). Unique mineral assemblages of shock-induced titanium-rich melt pockets in eucrite Northwest Africa 8003. *Geochemistry*, *79*, 125541. <https://doi.org/10.1016/j.chemer.2019.125541>
- Pang, R. L., Zhang, A. C., Wang, S. Z., Wang, R. C., & Yurimoto, H. (2016). High-pressure minerals in eucrite suggest a small source crater on Vesta. *Scientific Reports*, *6*, 26063. <https://doi.org/10.1038/srep26063>
- Rucks, M. J., Glotch, T. D., Whitaker, M. L., Sharp, T. G., Lindsley, D., Catalano, T., et al. (2019). The behavior of calcium-rich plagioclase under impact relevant conditions and implications for impact studies. In *50th Lunar and Planetary Science Conference Abstract#2691*.

- Rucks, M. J., Whitaker, M. L., Glotch, T. D., Parise, J. B., Jaret, S. J., Catalano, T., et al. (2018). Making Tissintite: Mimicking Meteorites in the Multi-Anvil. *American Mineralogist*, *103*, 1516–1519. <https://doi.org/10.2138/am-2018-6539>
- Schaal, R. B., & Hörz, F. (1980). Experimental shock metamorphism of lunar soil. *Proceedings of the Lunar and Planetary Science Conference*, *2*, 1679–1695.
- Sharp, T. G., & DeCarli, P. S. (2006). Shock effects in meteorites. *Meteorites and the Early Solar System II*. (pp. 653–677). Arizona: The University of Arizona Press.
- Simon, S. B., Davis, A. M., Grossman, L., & McKeegan, K. D. (2002). A hibonite-corundum inclusion from Murchison: A first-generation condensate from the solar nebula. *Meteoritics & Planetary Sciences*, *37*, 533–548. <https://doi.org/10.1111/j.1945-5100.2002.tb00837.x>
- Spray, J. G. (2016). Lithification mechanisms for planetary regoliths: The glue that binds. *Annual Review of Earth and Planetary Sciences*, *44*, 139–174. <https://doi.org/10.1146/annurev-earth-060115-012203>
- Stöffler, D., Hamann, C., & Metzler, K. (2018). Shock metamorphism of planetary silicate rocks and sediments: Proposal for an updated classification system. *Meteoritics & Planetary Sciences*, *53*, 5–49. <https://doi.org/10.1111/maps.12912>
- Takigawa, A., Stroud, R. M., Nittler, L. R., Alexander, C. M. O. D., & Miyake, A. (2018). High-temperature dust condensation around an AGB star: Evidence from a highly pristine presolar corundum. *The Astrophysical Journal Letters*, *862*, L13. <https://doi.org/10.3847/2041-8213/aad1f5>
- Tomeoka, K., Yamahana, Y., & Sekine, T. (1999). Experimental shock metamorphism of the Murchison CM carbonaceous chondrite. *Geochimica et Cosmochimica Acta*, *63*, 3683–3703. [https://doi.org/10.1016/S0016-7037\(99\)00149-0](https://doi.org/10.1016/S0016-7037(99)00149-0)
- Tomioaka, N., & Miyahara, M. (2017). High-pressure minerals in shocked meteorites. *Meteoritics & Planetary Sciences*, *52*, 2017–2039. <https://doi.org/10.1111/maps.12902>
- Walton, E. L., Sharp, T. G., Hu, J., & Filiberto, J. (2014). Heterogeneous mineral assemblages in Martian meteorite Tissint as a result a recent small impact event on Mars. *Geochimica et Cosmochimica Acta*, *140*, 334–348. <https://doi.org/10.1016/j.gca.2014.05.023>
- Wünnemann, K., Collins, G. S., & Osinski, G. R. (2008). Numerical modeling of impact melt production in porous rocks. *Earth and Planetary Science Letters*, *269*, 530–539. <https://doi.org/10.1016/j.epsl.2008.03.007>
- Xie, Z. D., Sharp, T. G., & DeCarli, P. S. (2006). Estimating shock pressure based on high-pressure minerals in shock-induced melt veins of L chondrites. *Meteoritics & Planetary Sciences*, *41*, 1883–1898. <https://doi.org/10.1111/j.1945-5100.2006.tb00458.x>
- Xing, W., Lin, Y., Zhang, C., Zhang, M., Hu, S., Hofmann, B. A., et al. (2020). Discovery of reidite in the lunar meteorite Sayh al Haymir 169. *Geophysical Research Letters*, *47*, e2020GL089583. <https://doi.org/10.1029/2020GL089583>
- Yamaguchi, A., & Sekine, T. (2000). Monomineralic mobilization of plagioclase by shock: An experimental study. *Earth and Planetary Science Letters*, *175*, 289–296. [https://doi.org/10.1016/S0012-821X\(99\)00299-X](https://doi.org/10.1016/S0012-821X(99)00299-X)
- Yang, J., Zhang, C., Miyahara, M., Tang, X., Gu, L., & Lin, Y. (2019). Evidence for early impact on a hot differentiated planetesimal from Al-rich micro-inclusions in ungrouped achondrite Northwest Africa 7325. *Geochimica et Cosmochimica Acta*, *258*, 310–335. <https://doi.org/10.1016/j.gca.2019.03.010>
- Zhang, A. C., Hsu, W. B., Floss, C., Li, X. H., Li, Q. L., Liu, Y., et al. (2010). Petrogenesis of lunar meteorite Northwest Africa 2977: Constraints from in situ microprobe results. *Meteoritics & Planetary Sciences*, *45*, 1929–1947. <https://doi.org/10.1111/j.1945-5100.2010.01131.x>
- Zhang, A. C., Hsu, W. B., Li, X. H., Ming, H. L., Li, Q. L., Liu, Y., et al. (2011). Impact melting of Dhofar 458 lunar meteorite: Evidence from polycrystalline texture and decomposition of zircon. *Meteoritics & Planetary Sciences*, *46*, 103–115. <https://doi.org/10.1111/j.1945-5100.2010.01144.x>

Reference From the Supporting Information

- Lafuente, B., Downs, R. T., Yang, H., & Stone, N., (2015). The power of databases: The RRUFF project. In T. Armbruster, & R. M. Danisi (Eds.), *Highlights in Mineralogical Crystallography* (pp. 1–30). Berlin: Walter de Gruyter GmbH.